Nuclear Instruments and Methods in Physics Research B 382 (2016) 54–59

Contents lists available at ScienceDirect

Nuclear Instruments and Methods in Physics Research B

journal homepage: www.elsevier.com/locate/nimb

Ion transport through macrocapillaries – Oscillations due to charge patch formation

D.D. Kulkarni [a], L.A.M. Lyle [b], C.E. Sosolik [a,*]

[a] Department of Physics and Astronomy, Clemson University, Clemson, SC 29634, USA
[b] Department of Physics, University at Buffalo, The State University of New York, Buffalo, NY 14260, USA

ARTICLE INFO

Article history:
Received 22 February 2016
Received in revised form 29 March 2016
Accepted 1 April 2016
Available online 19 April 2016

Keywords:
Ion-transport
Macrocapillary
Guiding
Charge patch formation

ABSTRACT

We present results on ion transport through large bore capillaries (macrocapillaries) that probe both the geometric and ion-guided aspects of this ion delivery mechanism. We have demonstrated that guiding in macrocapillaries exhibits position- and angle-dependent transmission properties which are directly related to the capillary material (either metal or insulator) and geometry. Specifically, we have passed 1 keV Rb^+ ions through glass and metal macrocapillaries, and have observed oscillations for the transmitted ion current passing through the insulating capillaries. Straightforward calculations show that these oscillations can be attributed to beam deflections from charge patches that form on the interior walls of the capillary. The absence of these oscillations in the metal capillary data serve as further confirmation of the role of charge patch formation.

1. Introduction

Multiply/Highly charged ions (M/HCIs) are unique in the field of ion-related physics as their charge state is significantly higher than the traditional singly-charged ions which dominate the field. This charge state, which is manifest as a non-negligible potential energy of the ions, can be used to modify the surface/subsurface structure of materials in ways that are distinct from other forms of radiation [1–6]. Beams of M/HCIs are obtained from sources such as Electron Beam Ion Source/Traps (EBIS/Ts) and Electron Cyclotron Resonance (ECR) ion sources in laboratories worldwide [7–14] and most recently at our own user facility for surface modification [15] as well as medical physics [16]. Despite this access, a major hurdle in effectively harnessing the potential of these beams for industrial environments is efficient and flexible ion-transport technology.

One approach towards non-conventional ion transport that has garnered significant attention over the last two decades is the use of capillaries as ion guides. In 2002, Stolterfoht et al. observed the so-called "guiding effect" in insulating capillaries [17]. This effect involves charge patch formation on the inside walls of the insulating capillary due to neutralization of and secondary electron emission initiated by the colliding M/HCI beam. Although these charges formed on the wall can dissipate into the capillary bulk or along the surface, they can also interact repulsively with ions of the incoming M/HCI beam to deflect them away from the capillary wall. After sufficient time has elapsed, a steady-state condition can be reached between charge patch formation and charge dissipation such that a charge-state and kinetic energy preserving transmission of the M/HCI beam is established. This is the definition of the guiding effect for ions within a capillary, and an extensive review of the existing research in this field can be found in Ref. [18].

Existing research can be classified into two categories depending on the diameter d of the capillaries used for guiding: nanocapillaries ($d < 1\mu m$) and macrocapillaries ($d > 1\mu m$) [19]. Recent efforts in macrocapillary transport include the use of external electric fields to guide the ions in conjunction with the guiding effect to improve efficiency of transport [20], use of conical capillaries for guiding antiparticle beams [21] and the use of curved glass capillaries to achieve large bending angles [22]. In this paper, we have studied the transport of singly-charged ions through straight and conical sections of insulating as well as metallic macrocapillaries. Our goal was to measure and understand the position- and angle-dependent characteristics of ion transport through these macrocapillaries.

The organization of this paper is as follows. In Section 2 we describe the experimental setup used in these measurements. In Section 3, we present data measured on a cylindrical metallic, a cylindrical insulating and a conical insulating macrocapillary. Differences and similarities in the data are noted and used to draw conclusions regarding charging effects, which are summarized in Section 4.

* Corresponding author.
E-mail address: sosolik@clemson.edu (C.E. Sosolik).

http://dx.doi.org/10.1016/j.nimb.2016.04.004
0168-583X/

2. Experiment

We have measured the position- and angle-dependent transmission properties of singly-charged ions for macrocapillaries with diameters and lengths of a few millimeters and a few centimeters respectively. The experiment was conducted at Clemson University using the singly charged ion beamline described in detail in Ref. [23]. An aluminosilicate emitter (HeatWave Labs, Inc.) was installed as the ion source in the beamline to obtain Rb^+ ions. The kinetic energy of the Rb^+ ions was fixed at 1 keV for all measurements. The energy spread of the beam is less than 1% [24].

Macrocapillaries of two types were used in this study: metals (stainless steel) and insulators (glass). The dimensions of the capillaries are shown in Table 1. The inlet refers to the side of the capillary through which the ions were incident, while the outlet is the exit side of the capillary. The critical angle θ_c is defined as the maximum angle of the capillary with respect to the incident beam of ions for which geometric transmission is possible. This angle is equivalent to the angle made by a line that touches the farthest and opposite corners in a length-wise cross-section of a capillary and is given by $\theta_c = \tan^{-1}((d_{in} + d_{out})/2l)$. We note that for our study, all capillaries were cylindrical ($d_{in} = d_{out}$) except one conical capillary denoted by Sample # 4 which had a taper of $4.52° \pm 0.12°$.

Before inserting the capillaries into our vacuum system, they were cleaned using standard UHV procedures, i.e. ten minute cycles of sonication with soap-water, acetone, and ethanol interspersed with rinsing in distilled water. Each macrocapillary was then mounted in a custom vacuum chamber inserted immediately after our Colutron G2 ion source [25]. The typical pressure in the chamber for these measurements was $\sim 1 \times 10^{-8}$ Torr. The macrocapillaries were secured along the beamline axis on a rotary feedthrough mounted on a linear translator. The translator allowed us to move the capillary perpendicular to the path of the beam to measure position dependent characteristics, while the rotary feedthrough allowed us to change the incident angle of the incoming ions relative to the capillary inlet. Each capillary was mounted with an adhesive metal tape on the exposed edge of the inlet to avoid entrance charging effects. The space around the capillary was shielded using a metal foil held in place by metal adhesive tape. The shield was necessary to ensure that only those ions that passed through the inside of the capillary and not around it were detected in these measurements.

A Faraday cup located ~15 cm downstream from the capillary mounting was used to measure the current of ions transmitted through the capillaries. For each measurement, the Rb^+ ion beam was tuned into the Faraday cup with the capillary retracted from the beam path. The capillary was then inserted into the path of the beam and the cup current was monitored to determine the insertion distance at which transmission of ions through the capillary was maximized. In addition, the insertion distances (on either side of this maximum point) at which the measured transmission through the capillary was zero were also recorded. Following these baseline measurements, the transmitted current was monitored as a function of time at multiple distances between the zero measurement end-points to obtain position-dependent characteristics (see, *e.g.* Fig. 1a). Angle-dependent characteristics for each capillary were obtained at the insertion distance of maximum transmission by varying the angle in steps of ~0.2°–0.3° and monitoring the transmitted current as a function of time (see, *e.g.* Fig. 1b). For these position- and angle-dependent measurements, the transmitted current through the metal and insulating capillaries was recorded in time steps of ~15 s and ~500 s respectively. Insertion distances were measured using a Vernier caliper (±0.1 mm), while a digital sensor connected to a PC was used to measure angles (±0.09°). The Faraday cup was connected to a Keithley 617 electrometer interfaced to a computer via GPIB for automated measurements. To improve the current measurement precision, the connection points for the Faraday cup were sanded down and connected using extremely short cables to reduce capacitive losses and the electrometer power connection was isolated from other laboratory connections to minimize AC pick-up. These steps resulted in a precision of ±5 pA for our measurements of transmitted current.

Table 1
Table showing the material, length (l), inlet diameter (d_{in}), outlet diameter (d_{out}) and critical angle (θ_c) for the various macrocapillaries used in this experiment. The uncertainties associated with these dimensions are ±0.1 mm and ±0.12°.

Sample #	Material	l (mm)	d_{in} (mm)	d_{out} (mm)	θ_c (°)
1	Steel	21.0	2.3	2.3	6.25
2	Glass	35.5	5.4	5.4	8.65
3	Glass	21.0	5.4	5.4	14.42
4	Glass	19.6	5.4	2.3	11.11

3. Results and discussion

Position- and angle-dependent data were obtained for the four macrocapillaries listed in Table 1 using the methods described in the previous section. Fig. 1 shows transmitted currents as a function of time measured for the metal capillary (Sample # 1). Each line in the figure refers to a measurement conducted when the capillary was inserted to a specific distance (Fig. 1a) or rotated to a specific angle (Fig. 1b) in the presence of the incident ion beam. In Fig. 1a, the positions E_1, E_2, and C refer to the insertion distances where the transmitted ion current through the capillary are zero (E_1 and E_2) or maximum (C). The up and down arrows in the figure indicate that as the capillary was moved away from the E_1/E_2 position or the C position, the transmitted current increased or decreased, respectively. For this metal macrocapillary these positions were $(E_1, E_2, C) = (0.0\text{ mm},\ 14.4\text{ mm},\ 7.2\text{ mm})$. These data indicate that the width of the incident ion beam was ~14 mm, which is much wider than the diameter of all of the capillaries used in this study. For the angular data shown in Fig. 1b, $\theta_{1,2}$ refer to the angles at which transmission dropped to zero while N refers to maximum transmission observed at normal incidence. As with the insertion data, the arrows on this figure refer to the increase or decrease of the transmitted current for rotations of the angle away from or toward the positions $\theta_{1,2}$ and N. For this metal macrocapillary the zero transmission angles were $(\theta_1, \theta_2) = (-6.12°, 7.02°)$, which lead to a measured critical angle $\theta_c = 6.57 \pm 0.09$ as compared to the theoretical value of 6.25°.

For the angular data of Fig. 1b, the maximum, minimum and mean transmitted current values measured at each angle were calculated and are plotted in Fig. 2. For this metal macrocapillary, these values are nearly equivalent and the plotted data lie on top of each other in the figure. For the glass capillaries (discussed below) this will no longer be the case. To understand the angular dependence shown in these data, we note that the tilt of the capillary modifies the effective opening area presented to the incident beam, as illustrated in Fig. 3 for a capillary of diameter d and length l. The functional form of this angular-dependent area, $A(\theta)$, is given by

$$A(\theta) = \frac{d^2}{2}\cos(\theta)[-\sin^{-1}(\gamma) + \gamma\cos(\sin^{-1}(\gamma)) + \pi/2] \quad (1)$$

where $\gamma = (l/d)tan(\theta)$.

The solid line in Fig. 2, which corresponds to this equation for our metal macrocapillary, shows that the measured angular-dependence of the transmitted current has a narrower angular

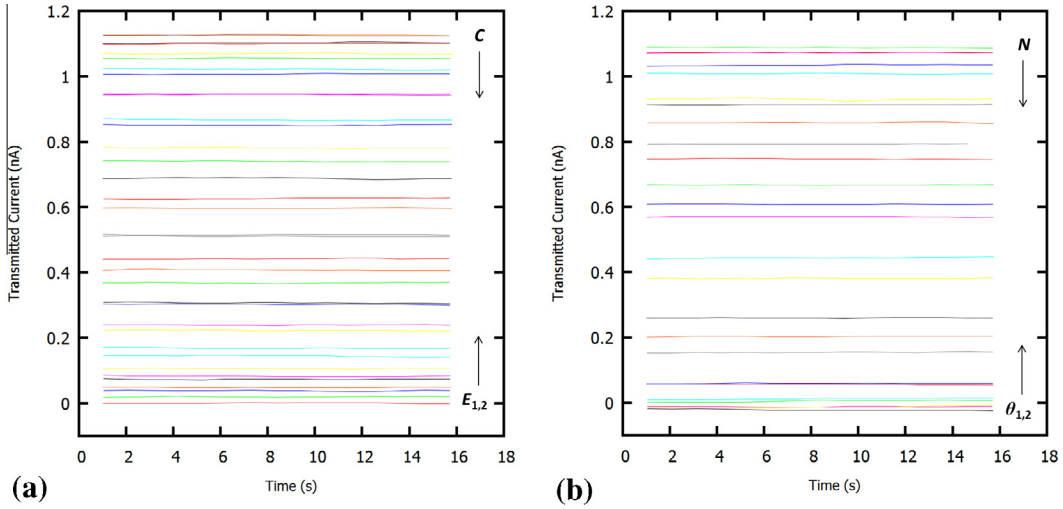

Fig. 1. (a) Position- and (b) angle-dependent raw data for the metal capillary (Sample # 1, l = 2.10 cm, $d_{in} = d_{out}$ = 0.23 cm). The transmitted current is plotted as a function of time at varying positions and angles. See text for details.

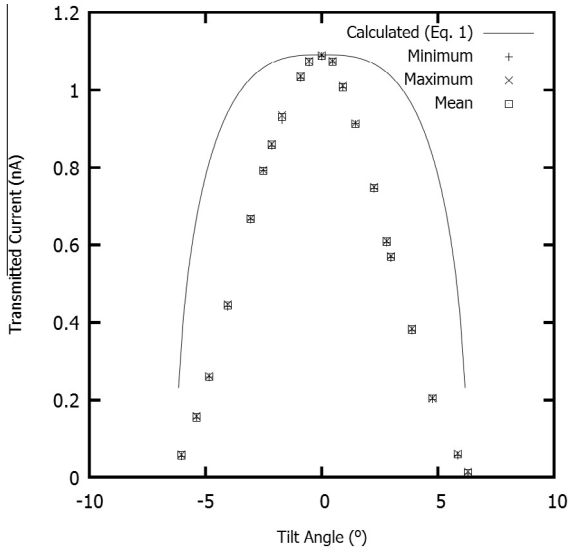

Fig. 2. Maximum, mean and minimum of transmitted current as a function of varying tilt angle for the metal capillary (Sample # 1, l = 2.10 cm, $d_{in} = d_{out}$ = 0.23 cm). The line shows the expected geometrical transmission from the capillary as a function of tilt angle.

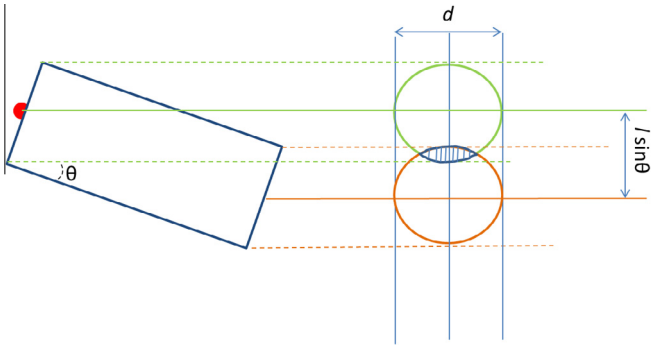

Fig. 3. Figure illustrating the varying area of the effective opening (hatched) as the capillary is tilted by an angle θ resulting in the observed angle-dependent characteristics for geometric transmission. An exact expression for this dependence is shown in Eq. (1) of the text.

range than this calculated geometrical limit. We note that our assumption of a constant current density and zero divergence for our incident ion beam could give rise to this discrepancy between the measured and calculated transmission values. For example, a Gaussian current density convolved with the functional form for $A(\theta)$ along with losses due to divergence would decrease the angular range of the calculated transmission. These corrections, which require more detailed incident ion beam measurements, will be pursued in future measurements.

Representative data for a straight glass macrocapillary (Sample # 2) is shown in Figs. 4 and 5. A comparison of the time-dependent results for the both the position (Fig. 4a) and tilt angle (Fig. 4b) with those discussed above for the metal macrocapillary (Fig. 1) reveals the primary difference between these capillary types, which is the oscillations in the transmitted current for the glass macrocapillary. Specifically. within the measurement ranges of $E_{1,2}$ and $\theta_{1,2}$ there are significant, time-dependent excursions in the transmitted current on a timescale of approximately one second. We note that the incident beam conditions for these capillary types (metal vs. insulating) was similar, which can be verified by examining the beam width and maximum transmitted current across the various measurements. For example, for these Sample # 2 data we obtained an ion beam width of ~14 mm, which is similar to the beam width determined for the metal macrocapillary (Sample # 1). In addition, the ratio of the maximum transmitted current in the metal and insulating capillaries (~5.48) is close to the ratio of the inlet area of the two capillaries (~5.51). Similar results were found for the other macrocapillaries listed in Table 1. Therefore, we conclude that the transmitted current excursions observed for the insulating macrocapillaries are material-dependent.

Fig. 5 shows the maximum, minimum and mean transmitted ion beam currents along with the calculated geometric transmission from Eq. (1) as a function of the corresponding tilt angles for the glass macrocapillary data shown in Fig. 4b. The angular spread for the maximum transmission is consistent with that predicted for geometric transmission. However, the angular spread for minimum, maximum and mean transmitted ion beam currents differs significantly. This can be seen by examining the critical angles for the maximum and minimum cases: $(\theta_{c,min}, \theta_{c,max})$ = (8.65°,2.83°).

In order to understand the results of Fig. 5, we first constrain our discussion to two angular ranges: $(\theta < \theta_{c,min})$ and $(\theta_{c,min} < \theta < \theta_{c,max})$. Within the first of these ranges, we see that

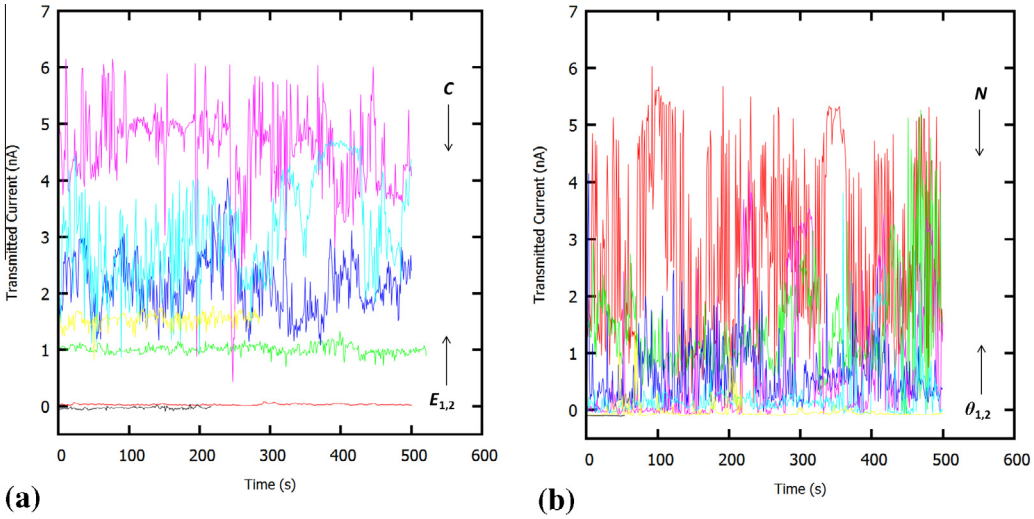

Fig. 4. (a) Position- and (b) angle-dependent raw data for an insulating capillary (Sample # 2, l = 3.55 cm, $d_{in} = d_{out}$ = 0.54 cm). The transmitted current is plotted as a function of time at varying positions and angles. See text for details.

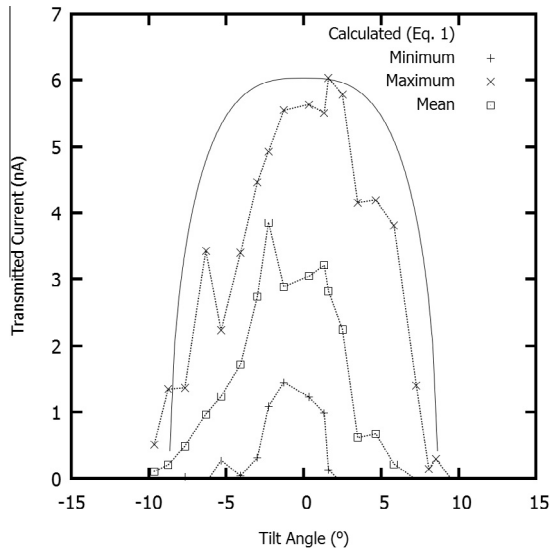

Fig. 5. Maximum, mean and minimum of transmitted current as a function of varying tilt angle for an insulating capillary (Sample # 2, l = 3.55 cm, $d_{in} = d_{out}$ = 0.54 cm). The solid line shows the expected geometrical transmission from the capillary as a function of tilt angle, while the dashed lines are drawn to guide the eye.

the minimum transmitted current is always non-zero. Therefore, we can interpret this as a region where ions are always transmitted regardless of time-dependent effects, *e.g.* charging of the walls. In the second angular range, we see that the minimum transmitted current is always zero, which implies that a time-dependent blocking of ion transmission is occurring. This variation or equivalently oscillation in the beam transmission may be linked to charge patch formation on the inside walls of the macrocapillary. It is well known that electric fields produced by charge patches can significantly affect the flight path of the ions. Similar oscillations in transmitted currents have been observed for glass macrocapillaries [26], Teflon macrocapillaries [27] and also for transmission through parallel glass plates [28]. In this context, our data indicate a preferential deflection of ions that pass closer to the walls as compared to the center of the capillary. That is, ions passing closest to the center of the capillary are not subjected to a deflection from electric fields originating from the capillary walls sufficient to make them escape detection. Conversely, those ions that are not near the center are more deflected such that they fall outside the range of detection and the minimum current falls to zero [29]. For the maximum transmitted current data shown in Fig. 5, we can interpret it as indicative of the time during which the walls of the macrocapillary have discharged and the deflection forces are no longer present. The similarities between these data and the metallic macrocapillary result (Fig. 2) then become obvious, as both are governed primarily by the geometric constraints of Eq. (1).

Although our data qualitatively point to beam deflection due to charge patch formation as the underlying origin of the observed oscillations of transmitted currents in insulating macrocapillaries, it is instructive to examine the order of magnitude of the fields required to give rise to it within our parameter space. Specifically, the kinetic energy of our incident ions is fixed at 1 keV, the path length to the Faraday cup detector is 15 cm, and the size of the detector is 2.54 cm. The distance and size of the detector together with the velocity of the ions set a constraint on the minimum electric field required to deflect the ions outside the detector's acceptance angle. For ions passing along the capillary axis, this electric field is calculated to be ~10 kV/m. The time taken to form such an electric field, assuming no discharge, is on the order of 1 s for the incident flux of our beam, which agrees well with the time period of our observed oscillations. Transport simulations utilizing classical phase-space dynamics for beam deflection along with temporal and spatial charge patch evolution are necessary for a detailed quantitative picture [30] of guiding; however, our calculation is sufficient to show that charge patch formation can give rise to our observed results.

Fig. 6 shows the transmitted currents as a function of time for the conical insulating macrocapillary (Sample # 4) where, as before, Fig. 6a and b show the position- and angle-dependent data, respectively. The oscillations in the transmitted ion current as a function of position are qualitatively similar to those seen in the straight insulating capillaries (Samples #2 and #3). The oscillations in the transmitted current as a function of angle, however, are significantly smaller in amplitude as compared to both the position-dependent transmission of the conical capillary itself and to the straight insulating capillaries in general. As a consequence, the maximum, mean and minimum of the transmitted current for the conical insulating macrocapillary appear much closer to each other, as shown in Fig. 7. We note that we have used the average radius for the calculated transmitted current as opposed to using

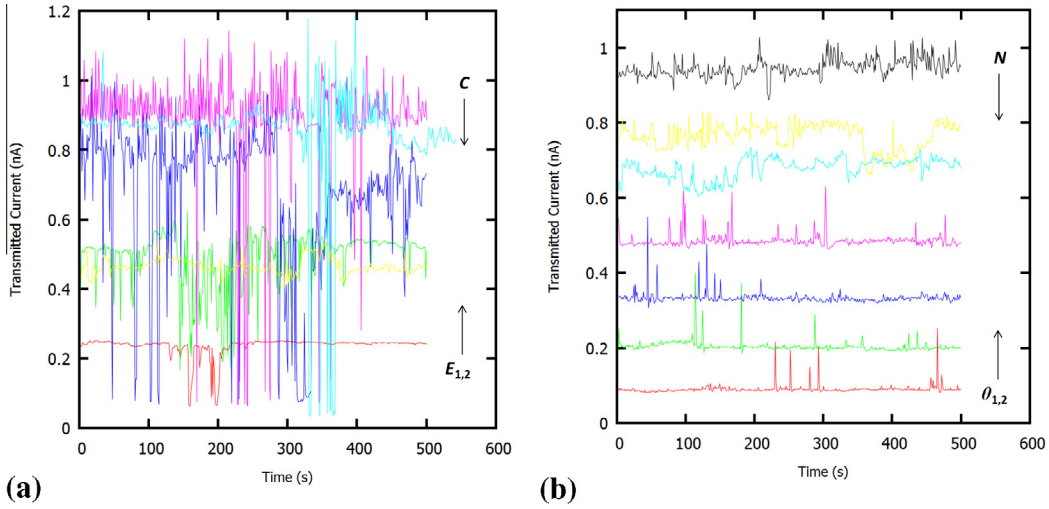

Fig. 6. (a) Position- and (b) angle-dependent raw data for the conical capillary (Sample # 4, l = 1.96 cm, d_{in} = 0.54 cm, d_{out} = 0.23 cm). The transmitted current is plotted as a function of time at varying positions and angles. See text for details.

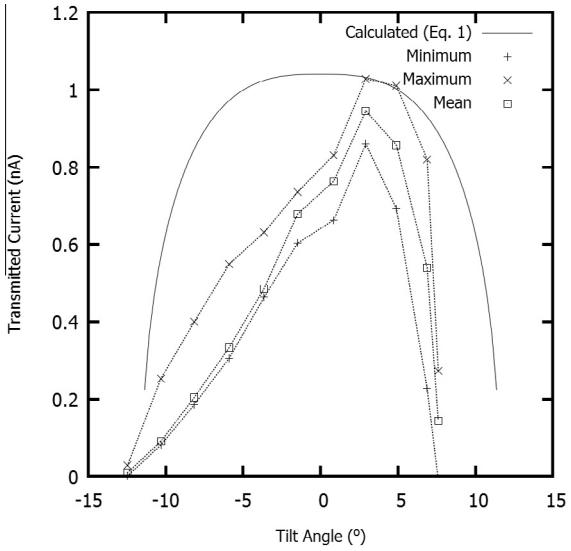

Fig. 7. Maximum, mean and minimum of transmitted current as a function of varying tilt angle for the conical insulating capillary (Sample # 4, l = 1.96 cm, d_{in} = 0.54 cm, d_{out} = 0.23 cm). The solid line shows the expected geometrical transmission from the capillary as a function of tilt angle, while the dashed lines are drawn to guide the eye.

a more general form of Eq. (1). The smaller amplitude of oscillation, or decreased variation in the maximum and minimum transmitted currents, indicates that charging effects were less pronounced for this macrocapillary.

4. Summary

We have measured the position- and angle-dependent transmission characteristics of 1 keV Rb^+ ions through metallic and insulating macrocapillaries. Transmission through the metal capillary was constant over time and no oscillations were observed in the recorded signal. The position-dependent data were used to calculate the beam width and also served to verify the stability of the beam over the duration of the experiment. The measured critical angles for transmission agreed well with those calculated from the geometry of the metal capillary, which implies that transmission through the capillary was consistent with straight-through line-of-sight transmission. For the insulating capillaries, the transmitted current was not constant and significant oscillations were observed that were absent in the case of the metal capillary. For a range of angles consistent with ion transmission parallel to the capillary axis, non-zero transmission was always observed; however, outside of this range (but within the geometrical critical angle) the transmission fell to zero intermittently. These observations indicate that electric fields due to charge patch formation preferentially deflect ions that are near the walls of the insulating macrocapillary. The absence of oscillations for the metal macrocapillary is consistent with this conclusion. In addition, a straightforward calculation involving the physical parameters of the setup shows that electric fields necessary to deflect the ions beyond the acceptance angle of the detector can form within the timescale of the observed oscillations.

Acknowledgments

The authors gratefully acknowledge financial support from the National Science Foundation (NSF-DMR-0960100), DARPA (ARO Grant No. W911NF-13–1-0042) and the Clemson University College of Engineering and Science. REU support for L.A.M. Lyle was provided by the National Science Foundation (NSF-EEC-1262991).

References

[1] T. Schenkel, A.V. Barnes, T.R. Niedermayr, M. Hattass, M.W. Newman, G.A. Machicoane, J.W. McDonald, A.V. Hamza, D.H. Schneider, Deposition of potential energy in solids by slow, highly charged ions, Phys. Rev. Lett. 83 (1999) 4273–4276.
[2] J.M. Pomeroy, A.C. Perrella, H. Grube, J.D. Gillaspy, Gold nanostructures created by highly charged ions, Phys. Rev. B 75 (2007) 241409.
[3] F. Aumayr, S. Facsko, A.S. El-Said, C. Trautmann, M. Schleberger, Single ion induced surface nanostructures: a comparison between slow highly charged and swift heavy ions, J. Phys. Condens. Matt. 23 (39) (2011) 393001.
[4] R.E. Lake, J.M. Pomeroy, H. Grube, C.E. Sosolik, Charge state dependent energy deposition by ion impact, Phys. Rev. Lett. 107 (2011) 063202.
[5] D.D. Kulkarni, R.E. Shyam, D.B. Cutshall, D.A. Field, J.E. Harriss, W.R. Harrell, C.E. Sosolik, Tracking subsurface ion radiation damage with metal-oxide-semiconductor device encapsulation, J. Mater. Res. 30 (2015) 1413–1421.
[6] T. Meguro, A. Hida, M. Suzuki, Y. Koguchi, H. Takai, Y. Yamamoto, K. Maeda, Y. Aoyagi, Creation of nanodiamonds by single impacts of highly charged ions upon graphite, Appl. Phys. Lett. 79 (23) (2001) 3866–3868.
[7] J.D. Gillaspy, First results from the EBIT at NIST, Phys. Scr. 1997 (T71) (1997) 99.
[8] R.E. Marrs, Recent results from the EBIT and super EBIT at Lawrence Livermore National Laboratory, Phys. Scr. 1997 (T73) (1997) 354.
[9] F. Meyer, M. Bannister, D. Dowling, J. Hale, C. Havener, J. Johnson, R. Juras, H. Krause, A. Mendez, J. Sinclair, A. Tatum, C. Vane, E.B. Musafiri, M. Fogle, R.

Rejoub, L. Vergara, D. Hitz, M. Delaunay, A. Girard, L. Guillemet, J. Chartier, The ORNL multicharged ion research facility upgrade project, Nucl. Instr. Meth. Phys. Res. Sect. B 242 (1–2) (2006) 71–78.
[10] E. Galutschek, R. Trassl, E. Salzborn, F. Aumayr, H. Winter, Compact 14.5 GHz all-permanent magnet ECRIS for experiments with slow multicharged ions, J. Phys. Conf. Ser. 58 (1) (2007) 395.
[11] G. Zschornack, S. Landgraf, F. Grossmann, U. Kentsch, V. Ovsyannikov, M. Schmidt, F. Ullmann, Dresden EBIT: the next generation, Nucl. Instr. Meth. Phys. Res. Sect. B 235 (1–4) (2005) 514–518.
[12] A.J.G. Martínez, J.R.C. López-Urrutia, D. Fischer, R.S. Orts, J. Ullrich, The Heidelberg EBIT: present results and future perspectives, J. Phys. Conf. Ser. 72 (1) (2007) 012001.
[13] Y. Fu, K. Yao, B. Wei, D. Lu, R. Hutton, Y. Zou, Overview of the Shanghai EBIT, J. Instrum. 5 (08) (2010) C08011.
[14] H. Watanabe, F. Currell, The Belfast EBIT, J. Phys. Conf. Ser. 2 (1) (2004) 182.
[15] R. Shyam, D.D. Kulkarni, D.A. Field, E.S. Srinadhu, D.B. Cutshall, W.R. Harrell, J. E. Harriss, C.E. Sosolik, First multicharged ion irradiation results from the CUEBIT facility at Clemson University, AIP Conf. Proc. 1640 (1) (2015) 129–135.
[16] D. Medlin, W. Heffron, A. Siegel, K. Wilson, A. Klingenberger, A. Gall, M. Rusin, D. Dean, E. Takacs, Development of an X-ray irradiation port for biomedical applications at the CUEBIT facility, J. Phys. Conf. Ser. 583 (1) (2015) 012048.
[17] N. Stolterfoht, J.-H. Bremer, V. Hoffmann, R. Hellhammer, D. Fink, A. Petrov, B. Sulik, Transmission of 3 keV Ne^{7+} ions through nanocapillaries etched in polymer foils: evidence for capillary guiding, Phys. Rev. Lett. 88 (2002) 133201.
[18] C. Lemell, J. Burgdörfer, F. Aumayr, Interaction of charged particles with insulating capillary targets – the guiding effect, Prog. Surf. Sci. 88 (3) (2013) 237–278.
[19] See Section 2.2 in Reference Aumayr-capillary-review.
[20] A. Wartak, R. Bereczky, G. Kowarik, K. Tőkési, F. Aumayr, Conceptual design and sample preparation of electrode covered single glass macro-capillaries for studying the effect of an external electric field on particle guiding, Nucl. Instr. Meth. Phys. Res. Sect. B 354 (2015) 324–327. 26th International Conference on Atomic Collisions in Solids.
[21] E. Giglio, R. DuBois, A. Cassimi, K. Tőkési, Low energy ion transmission through a conical insulating capillary with macroscopic dimensions, Nucl. Instr. Meth. Phys. Res. Sect. B 354 (2015) 82–85. 26th International Conference on Atomic Collisions in Solids..
[22] T.M. Kojima, T. Ikeda, Y. Kanai, Y. Yamazaki, Ion guiding in curved glass capillaries, Nucl. Instr. Meth. Phys. Res. Sect. B 354 (2015) 16–19. 26th International Conference on Atomic Collisions in Solids..
[23] M.P. Ray, R.E. Lake, S.A. Moody, V. Magadala, C.E. Sosolik, A hyperthermal energy ion beamline for probing hot electron chemistry at surfaces, Rev. Sci. Instr. 79 (2008) 076106.
[24] M. Menzinger, L. Wåhlin, High intensity, low energy spread ion source for chemical accelerators, Rev. Sci. Instrum. 40 (1) (1969) 102–105.
[25] See Figure 1 in reference Beamline.
[26] M. Alshammari, K. Alshammari, A. Cudd, R. DuBois, K. Tőkési, Exploring new aspects and practical applications of capillary guiding of charged particle beams, Nucl. Instr. Meth. Phys. Res. Sect. B 354 (2015) 20–22. 26th International Conference on Atomic Collisions in Solids.
[27] T.M. Kojima, T. Ikeda, Y. Kanai, Y. Yamazaki, V.A. Esaulov, Ion beam guiding with straight and curved Teflon tubes, J. Phys. D Appl. Phys. 44 (35) (2011) 355201.
[28] T. Ikeda, Y. Iwai, T.M. Kojima, S. Onoda, Y. Kanai, Y. Yamazaki, Resistive switching induced on a glass plate by ion beam irradiation, Nucl. Instr. Meth. Phys. Res. Sect. B 287 (2012) 31–34.
[29] E. Gruber, G. Kowarik, F. Ladinig, J.P. Waclawek, D. Schrempf, F. Aumayr, R.J. Bereczky, K. Tkési, P. Gunacker, T. Schweigler, C. Lemell, J. Burgdörfer, Temperature control of ion guiding through insulating capillaries, Phys. Rev. A 86 (2012) 062901.
[30] See Section 4 in reference Aumayr-capillary-review.